Near -IR interferometry:

spectrally dispersed *JHK*-band IOTA / GI2T interferograms, advantages of NIR, and aims

Gerd Weigelt

Max-Planck Institute for Radioastronomy, Bonn

Plan

- Interferometry with spectrally dispersed *JHK* interferograms (T Cep, CH Cyg, R CrB)
- IOTA FLUOR Interferometry (Miras)
- Advantages and aims of near-infrared interferometry

(other projects: VLTI VINCI, VLTI AMBER, LBT LINC)

MPIfR *JHK*-Band Beam Combiner Instrument

- Simultaneous recording of spectrally dispersed *J*-, *H*-, and *K*-band fringes (Weigelt et al. 2003, SPIE 4838, 181)
- Anamorphic, achromatic (JHK) cylindrical lens system and grism / prism spectrograph (similar to the visible GI2T beam combiner; Labeyrie et al. 1986, A&A 162, 359) and Hawaii camera.

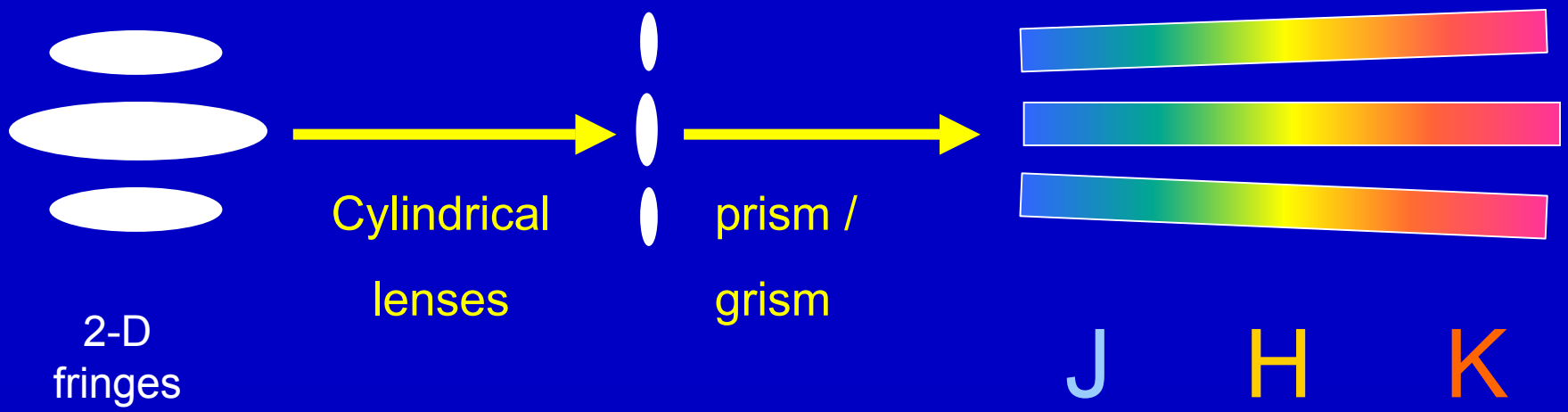

IOTA Spectro-Interferometry: First Spectrally Dispersed *JHK* Michelson Interferograms

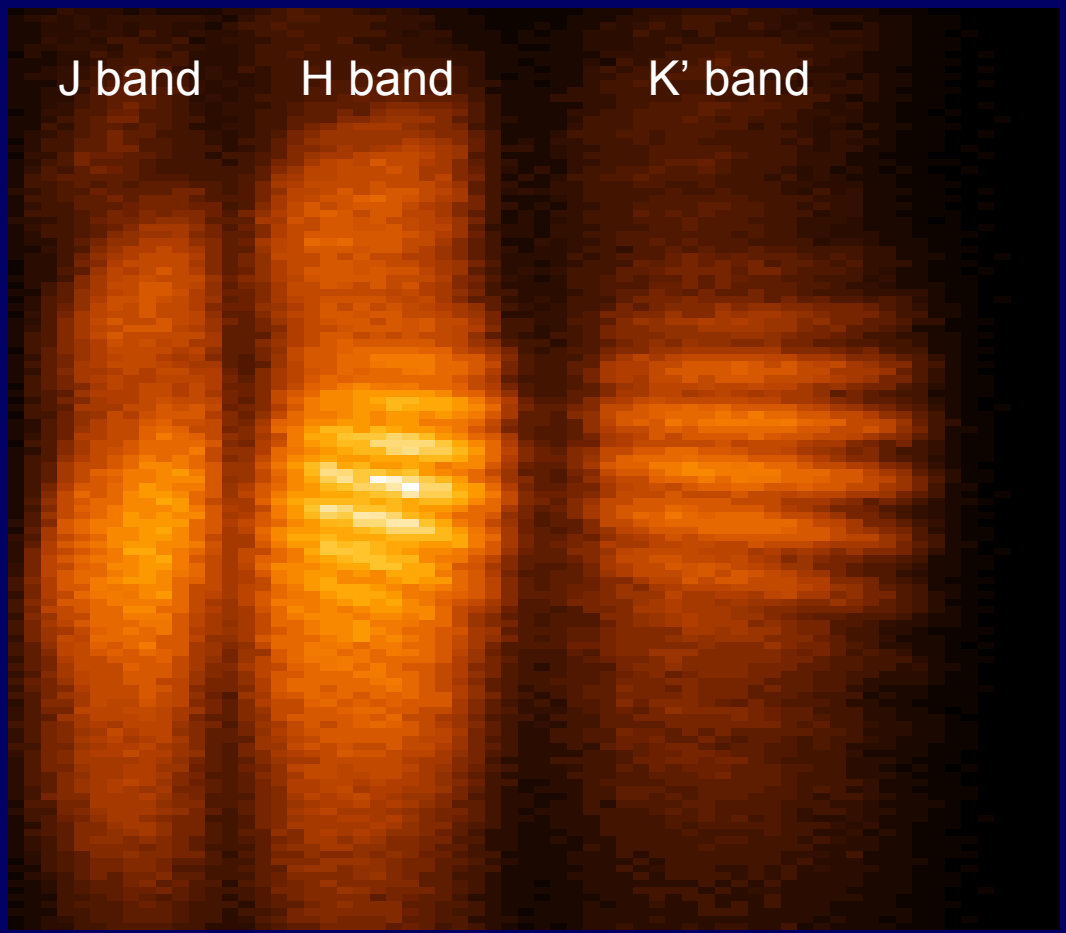

- T Cep
- 1-2.3 μm
- baseline 20 m
- IOTA

Spectrally dispersed GI2T Michelson interferograms:

wavelength range 1.9 - 2.4 μm

(Weigelt et al. 2000,

SPIE 4006, 617)

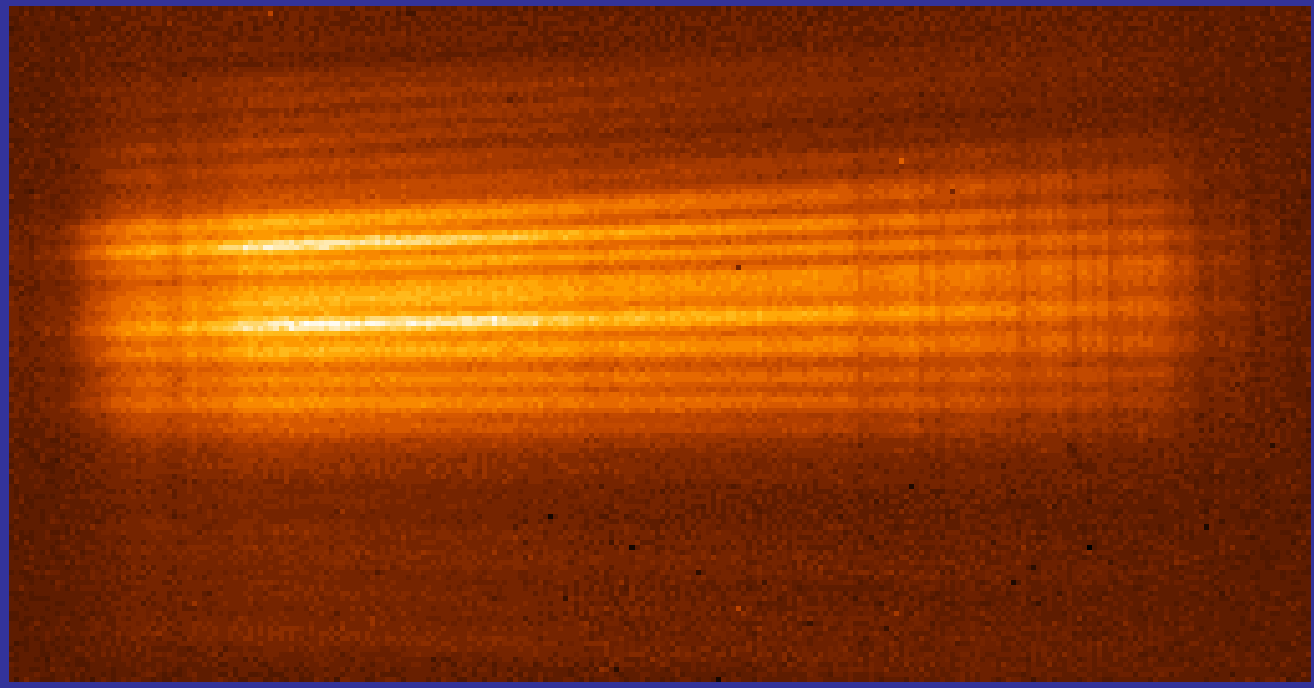

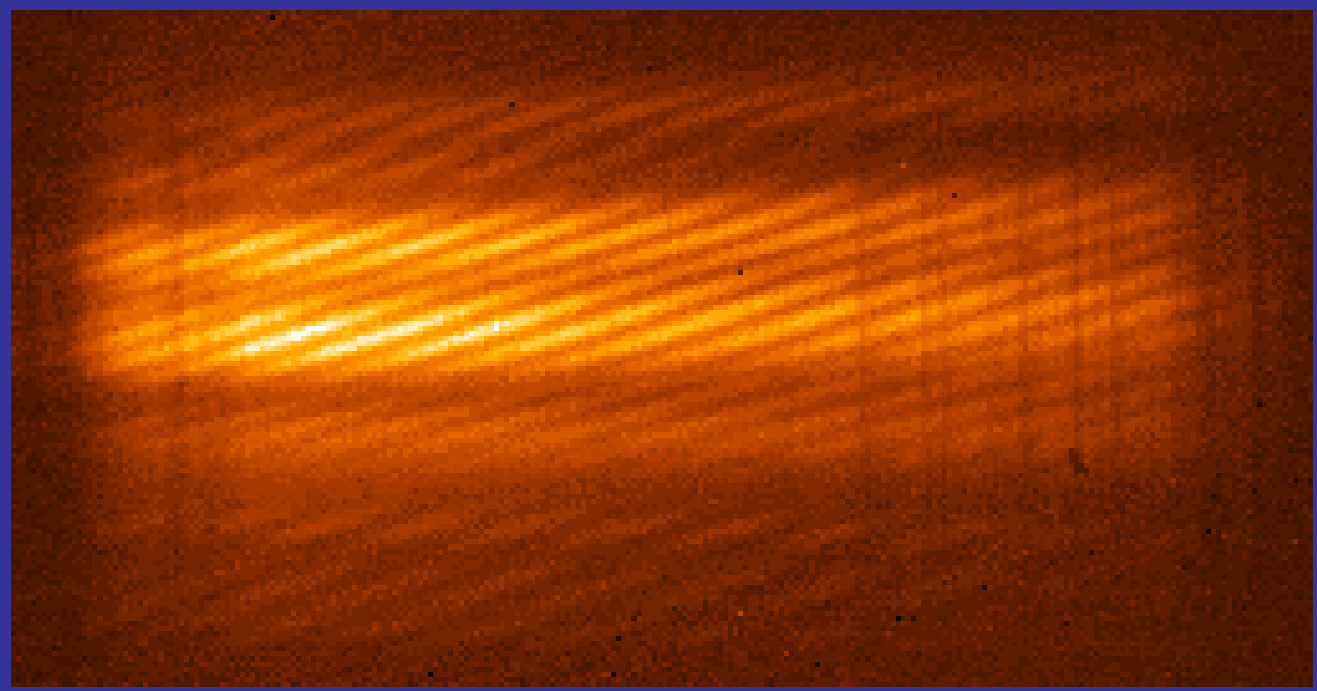

IOTA Observations: T Cep, CH Cyg, and R CrB

- Four baselines in the range of 14 m to 27 m; *J*, *H*, and *K* UD diameters
- Comparison of T Cep and CH Cyg observations with Mira models and derivation of Rosseland radii and effective temperatures
- R CrB: first resolution of its dust shell; radiative transfer modeling
- Measurements of visibility ratios $V(\lambda_1) / V(\lambda_2)$ for the investigation of the wavelength dependence of the T Cep diameter → $D(\lambda_1) / D(\lambda_2)$

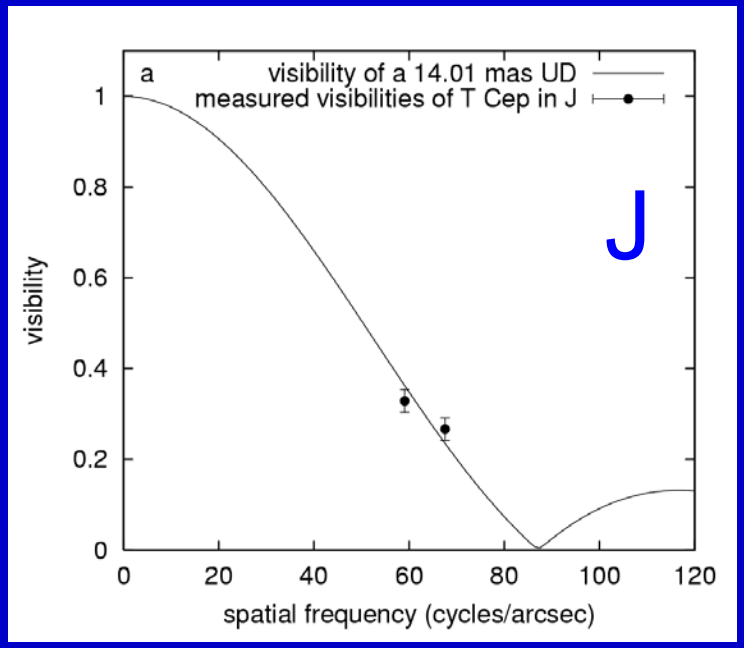

IOTA *JHK*-band interferometry of T Cep:

JHK Uniform-Disk Diameters:
14.0 +/- 0.6 mas
13.7 +/- 0.6 mas
15.0 +/- 0.6 mas
(Weigelt et al. 2003, SPIE 4838, 181)

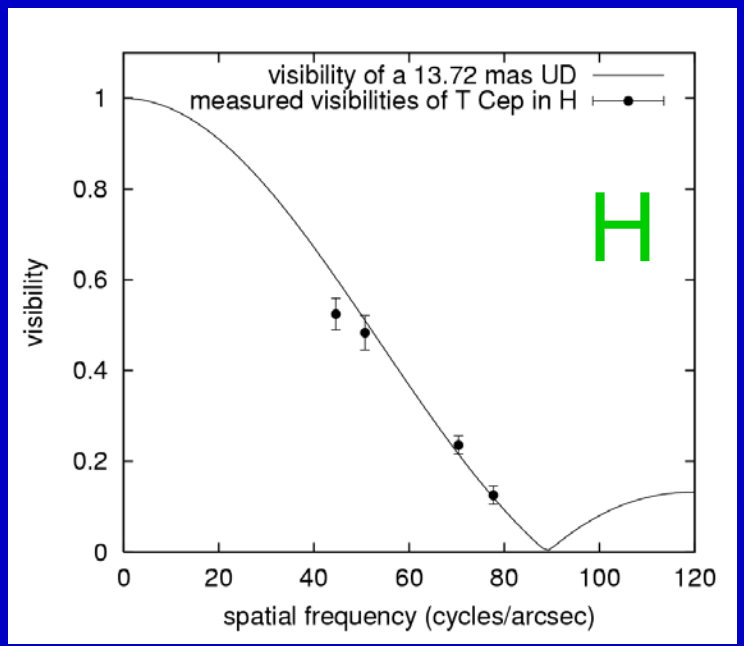

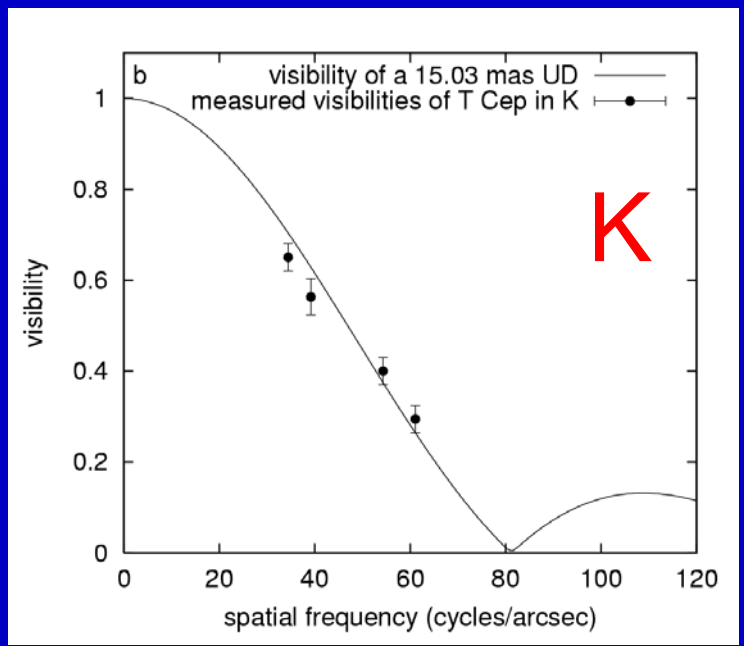

T Cep: Comparison of Observations with Models

- For the interpretation of the visibility measurements, detailed dynamic atmosphere models (Bessell, Scholz & Wood 1996; Hofmann, Scholz & Wood 1998) have to be taken into account which predict, for instance, diameters, model center-to-limb intensity variations (CLVs), and effective temperatur.

Advantages of comparison:

- (1) The comparison of measured stellar parameters (e.g. diameters, effective temperature, visibility shape) with theoretical parameters indicates whether any of the models is a fair representation of T Cep.

- (2) From the comparison of the observations with the models, fundamental stellar parameters can be derived.

Stellar Radii

Radii which are commonly used in theoretical studies and which we will derive:

- The monochromatic radius R_λ of a star at wavelength λ is given by the distance from the star's center to the layer where the optical depth τ =1.

- The stellar filter radius R_f is the corresponding intensity and filter weighted radius.

- The Rosseland radius R is given by the distance from the star's center to the layer at which the Rosseland optical depth equals unity.

- Principle of the derivation of radii: angular stellar radii (corresponding to different models) were determined by least-squares fits of the visibilities of model CLVs to the measured visibilities.

- Linear radii were derived from the angular radii by using the HIPPARCOS parallax of 4.76 +/- 0.75 mas (ESA 1997).

Linear *K*-Band Radii of T Cep: Comparison with Models

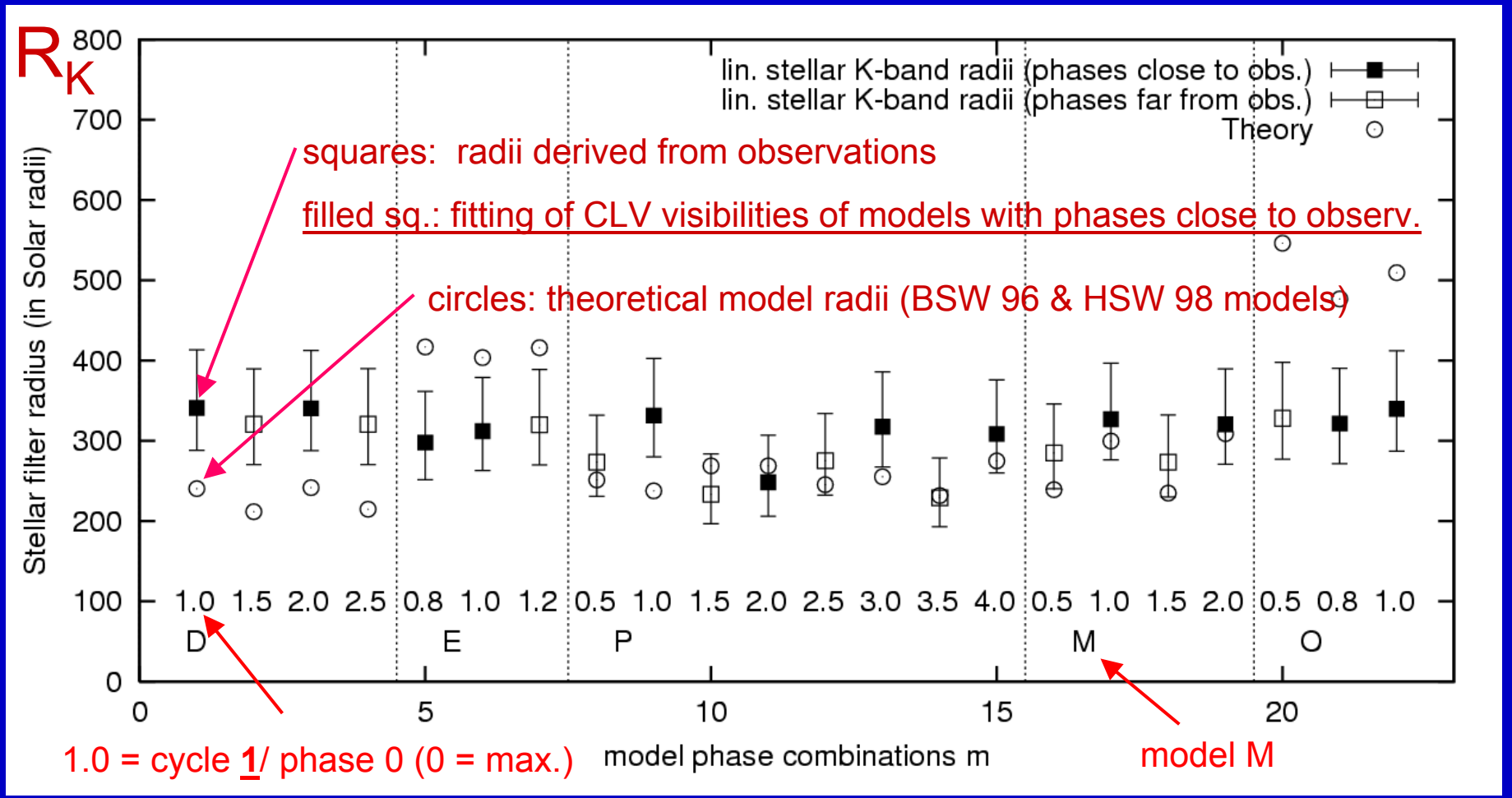

Rosseland radii were derived from the stellar filter radii and the theoretical ratios between the Rosseland and filter radii predicted by the models.

Comparison of the Radii Derived from the Observations with Theoretical Radii

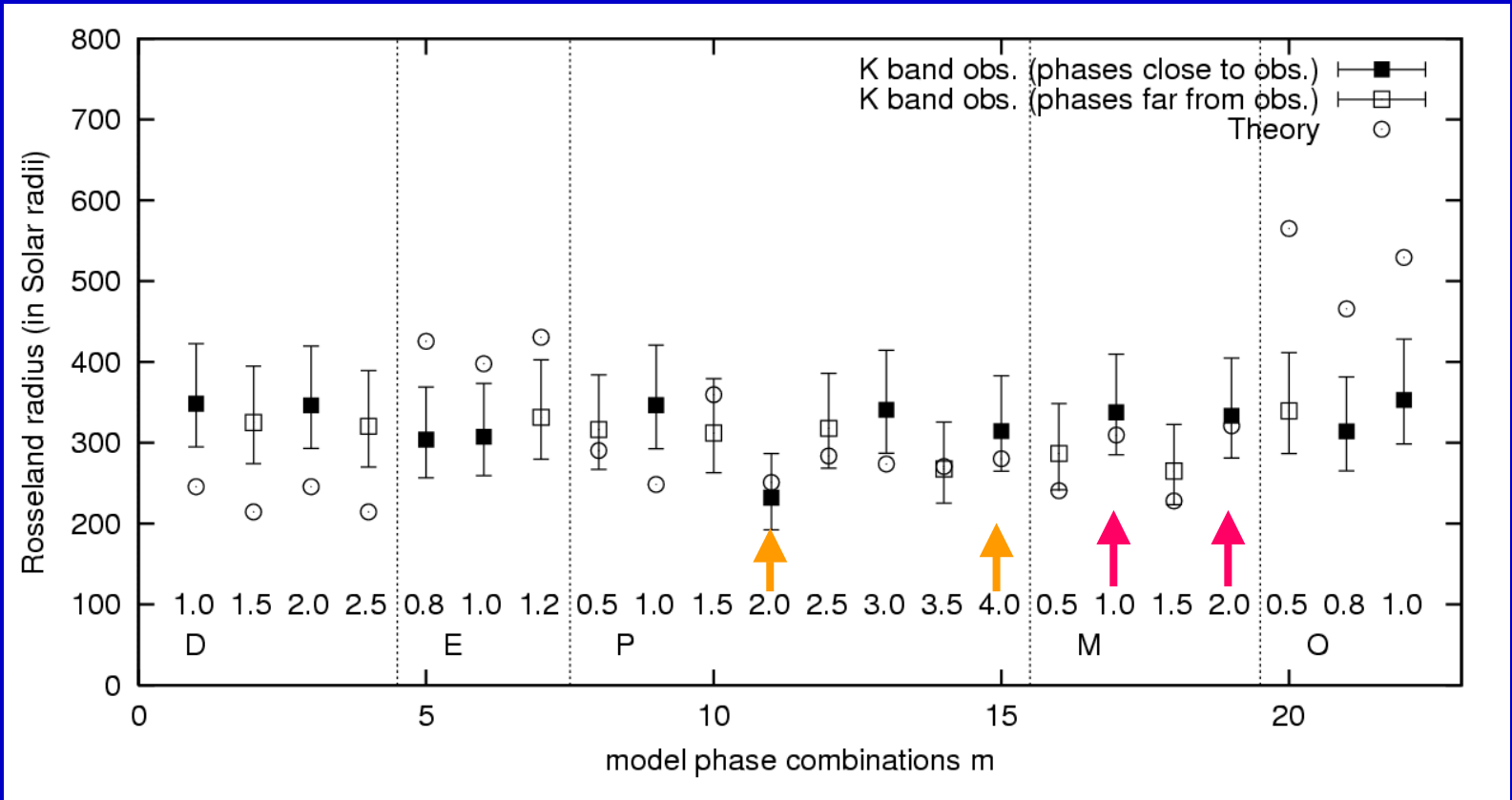

- Result: only the theoretical Rosseland radii of the fundamental mode M and P model are, at almost all near-maximum phases, close to the Rosseland radii derived from the observations. Comparison:
- M-model Rosseland radius derived from the observations: 335 +/- 70 solar radii; theoretical M-model Rosseland radius: 315 solar radii.

Effective Temperature of T Cep

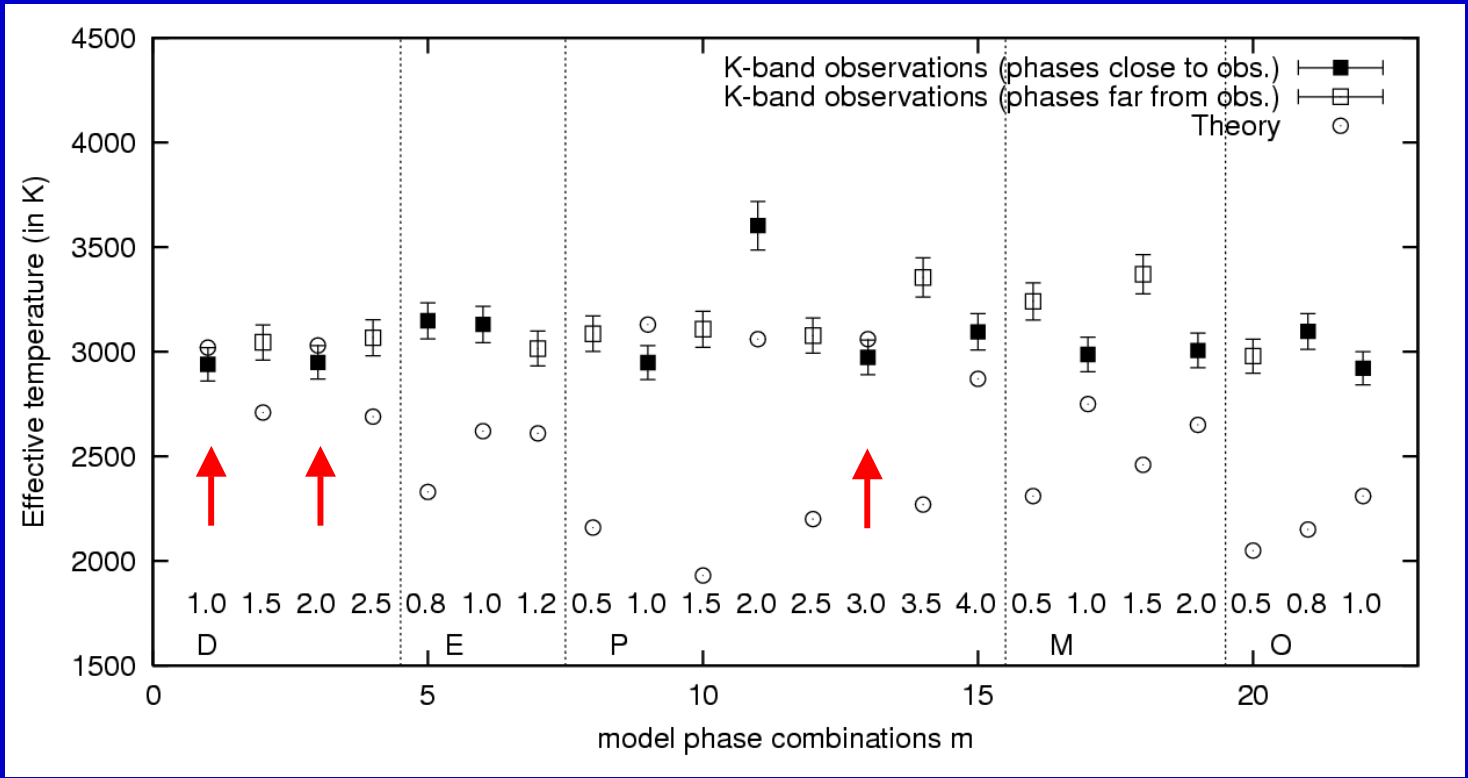

- T_{eff} was derived from the angular Rosseland radii and the bolometric flux obtained from *UBVJHKLM* photometry (Crimean Observatory). Bolometric flux: 593 10^8 erg cm^{-2} s^{-1}. Comparison:

  Theoretical P-model T_{eff} : 3030 K

  T_{eff} derived from observations (P model): 3150 +/- 90 K

T Cep: Diameter Ratios $D(\lambda_1) / D(\lambda_2)$

Our JHK interferograms allow the derivation of diameter ratios $D(\lambda_1) / D(\lambda_2)$ from visibility ratios $V(\lambda_1) / V(\lambda_2)$ and allow the comparison of the observed diameter ratios with theoretical model diameter ratios (Weigelt et al. 2003):

- The diameter ratios derived from our observations show that the diameter of T Cep is much larger at 2.03 μm than at 2.15 μm or 2.26 μm. Why? The large 2.03 μm diameter is probably caused by light emitted by absorbing water molecules in the outer atmosphere (Jacob and Scholz 2002):

$D_{2.03\ \mu m} / D_{2.26\ \mu m} = 1.26$ and $D_{2.15\ \mu m} / D_{2.26\ \mu m} = 1.08$.

- These diameter ratios are in good agreement both with theoretical ratios (e.g. Jacob & Scholz 2002; P and M models) and with observations by Thompson, Creech-Eakman & van Belle 2002.

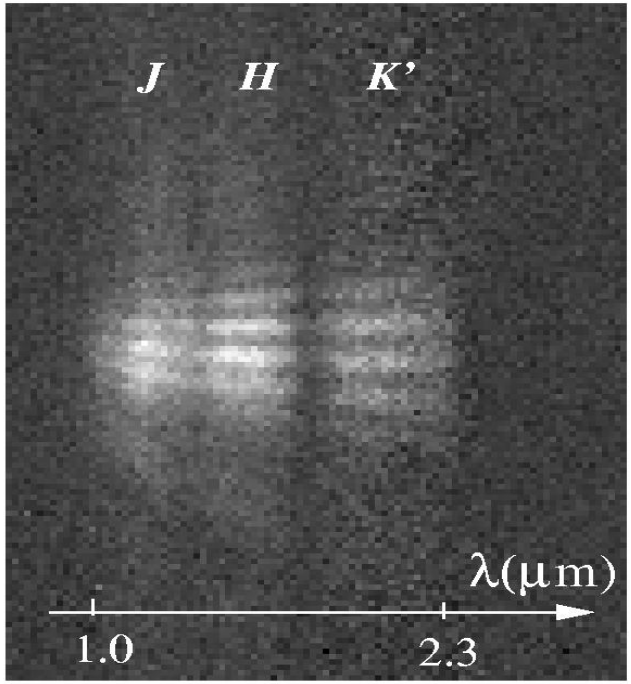

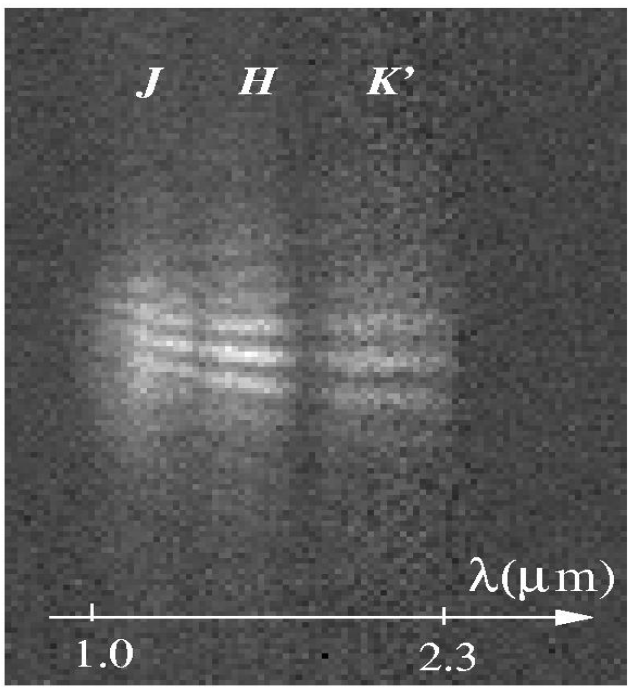

Resolution of the Dust Shell of R CrB

(Ohnaka et al. 2003, A&A 408, 553)

Table 1. IOTA observations for R CrB. B_p: projected baseline length, P.A.: position angle of the projected baseline, N_T: number of interferograms acquired for the target, N_R: number of interferograms acquired for the reference star, T: exposure time of each frame.

	2001 Jun. 05, 06
JD	2452067, 2452068
V (mag)	6
B_p	21.2 m
P.A.	167°
Spectral resolution ($\lambda/\Delta\lambda$)	~ 30
Reference star	HD 143393, HR 5877
N_T	7700
N_R	5000
T(ms)	300

JHK-band Interferometry and radiative transfer modeling of R CrB

SED + visibilities → physical parameters of the dust shell

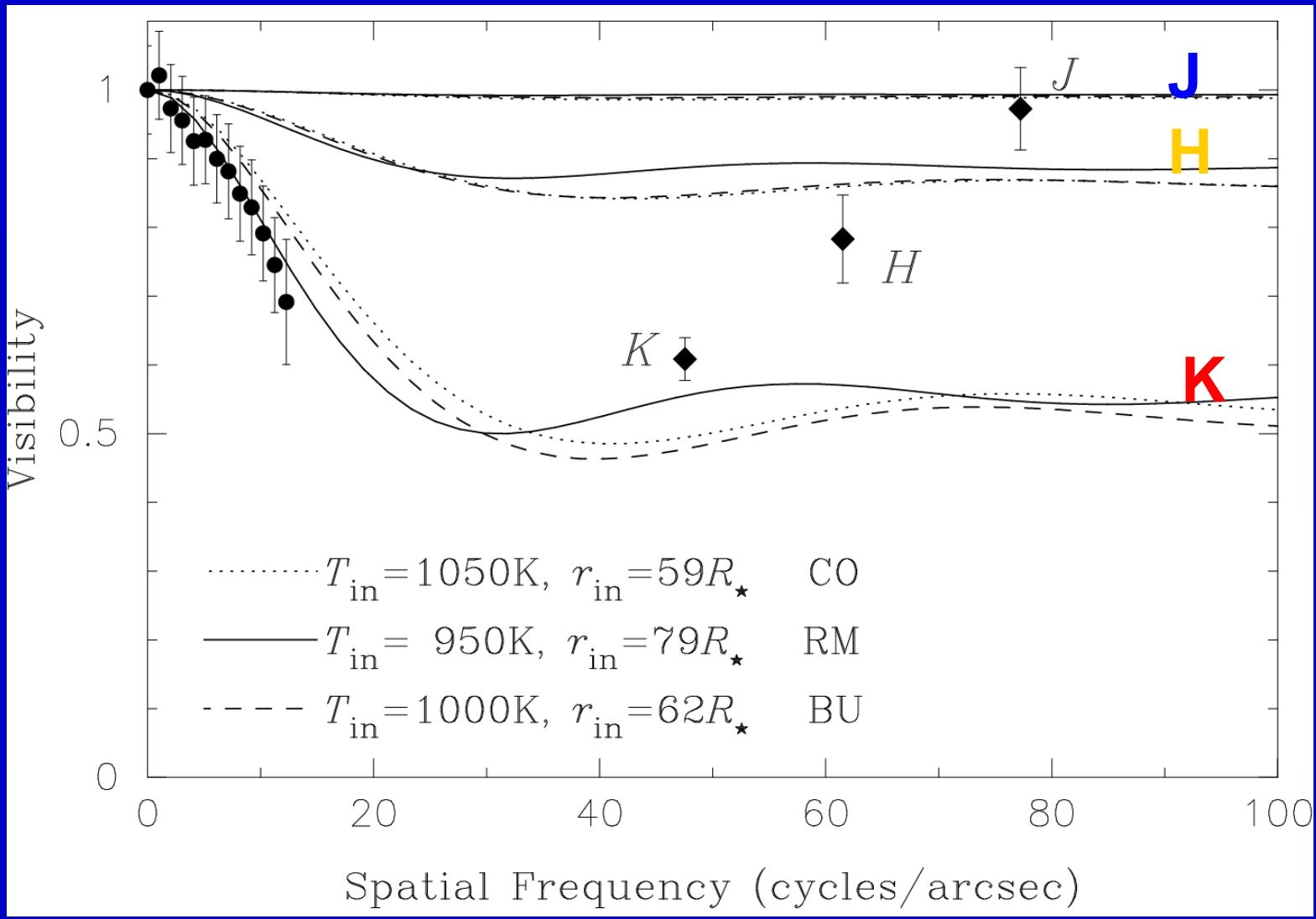

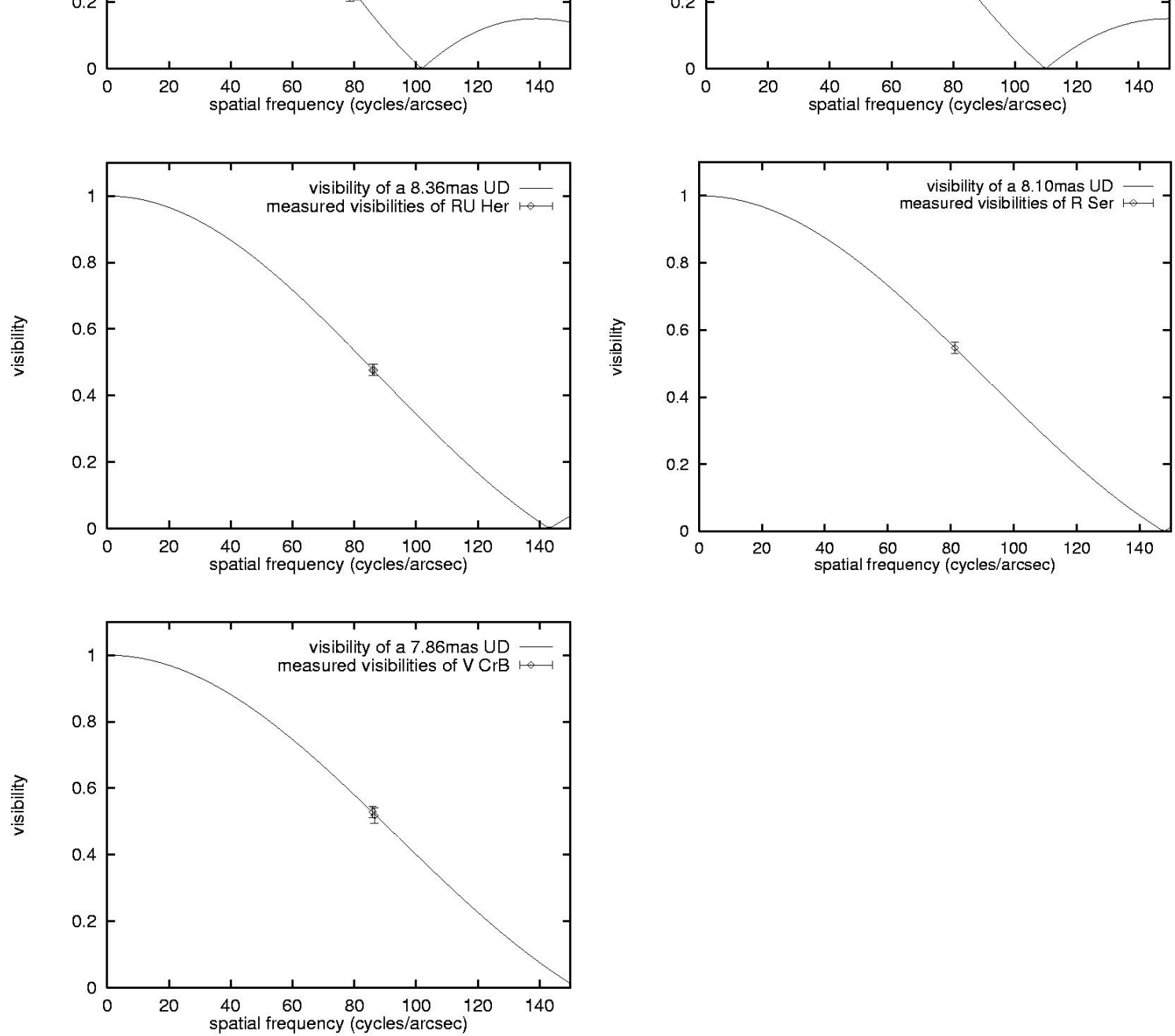

Fig. 1. Uniform-disk (UD) fits (X Oph, R Aql, RU Her, R Ser, and V CrB).

IOTA FLUOR observations of Mira stars

(Hofmann et al. 2002; New Ast. 7, 9)

Spatial fiber filters: IOTA FLUOR interferometry

(C. du Foresto & Ridgway 1992, ESO Proc. High-resolution Imaging by Interferometry II, p. 731; Mariotti et al. 1996, A&A Suppl. Ser. 116, 381)

IOTA FLUOR observations of R Aql

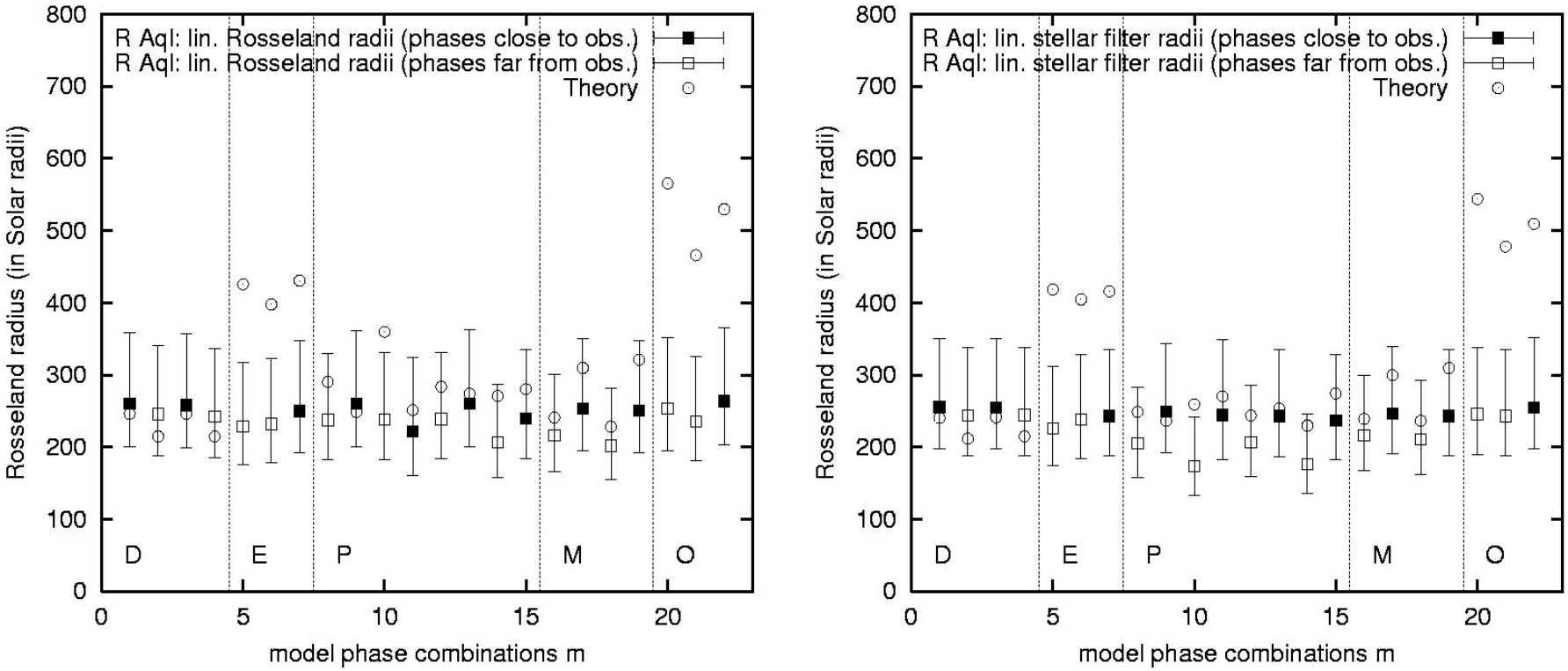

Fig. 2. Comparison of measured R Aql radii and theoretical model radii: (left) linear Rosseland radii $R_{\rm m}$ and (right) linear stellar K′-band radii $R_{\rm K',m}$ for all 22 model-phase combinations m. Measured linear radii derived from models *with phases close to our observations (= filled squares)* and far from our observations (open squares) are shown. The theoretical model radii are plotted with open circles. Table 3 gives the link between the abscissa values (model-phase combinations m) and the models and their phases.

VLTI phase-closure instrument AMBER

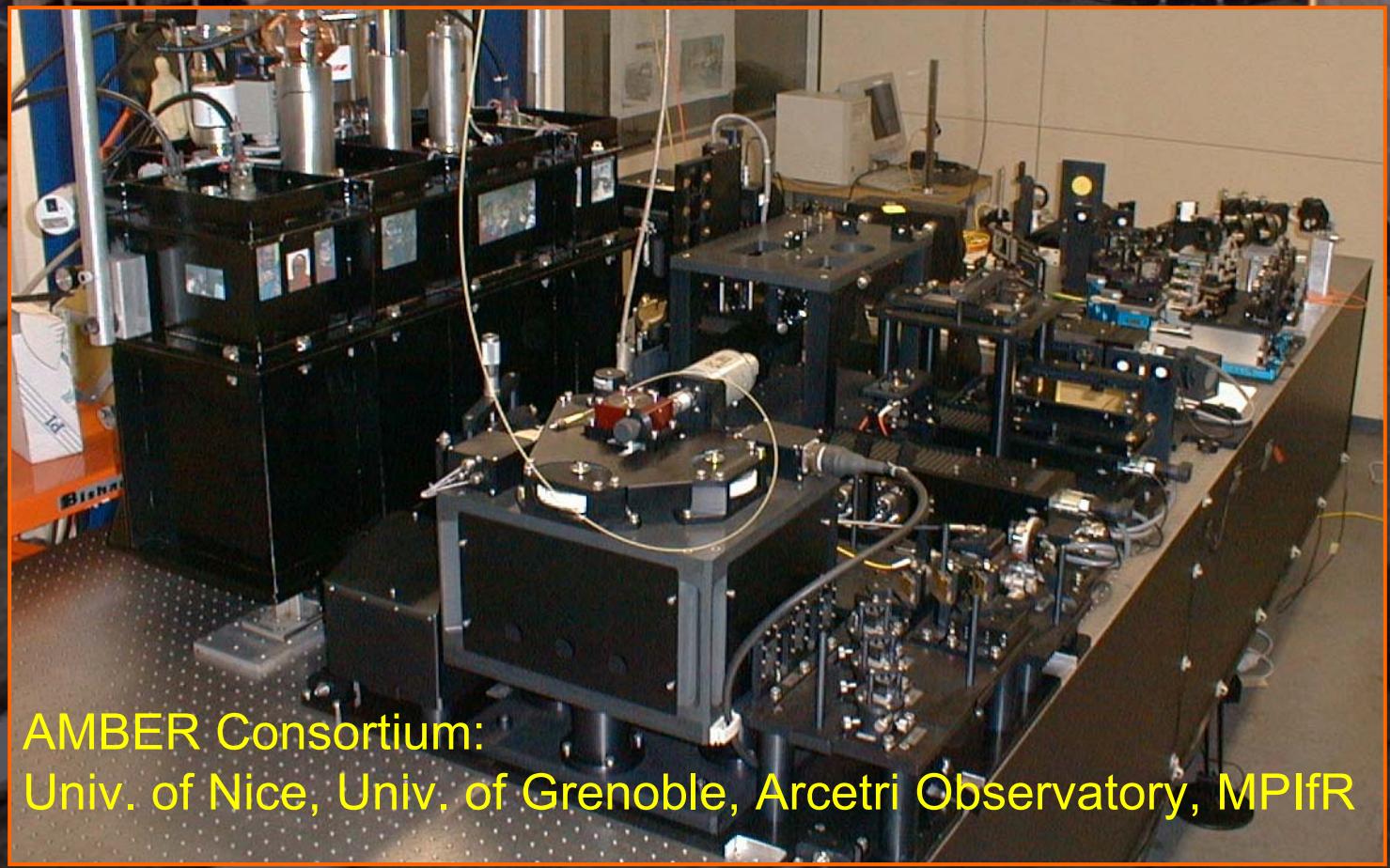

AMBER Consortium:
Univ. of Nice, Univ. of Grenoble, Arcetri Observatory, MPIfR

Advantages and aims of NIR interferometry: VLTI AMBER

- Resolution at wavelength 1 μm: 1 mas
- Limiting K magnitude / VLTI ATs: ~ 9
- Limiting K magnitude / VLTI UTs: ~ 12
- Visibility accuracy (fiber filters): ~ 0.1%
  λ-differential visibility accuracy: ~ 0.01%
- image reconstruction

- ***JHKN*** visibility + images + SED: 2D *JHKN* radiative transfer modeling
- 0.1-1% visibility accuracy: AGN tori, disks and jets of YSOs, …
- 0.01% accuracy of wavelength-differential visibility (emission lines/cont.): BLR (diameter ~ 0.1 mas), inner region of jets of YSO, exo-planets …

Illustration of the importance of *JHK-band and N*-band interferometry for radiative transfer modeling

Examples:

- Dust shell of the AGB star CIT 3
- Dust shell of the carbon star IRC +10216
- PPN Red Rectangle
- Massive YSO AFGL 2591 (dust sublimation radius and outflow)

SED + *JHKN* visibilities + JHK images → physical parameters of the dust shell

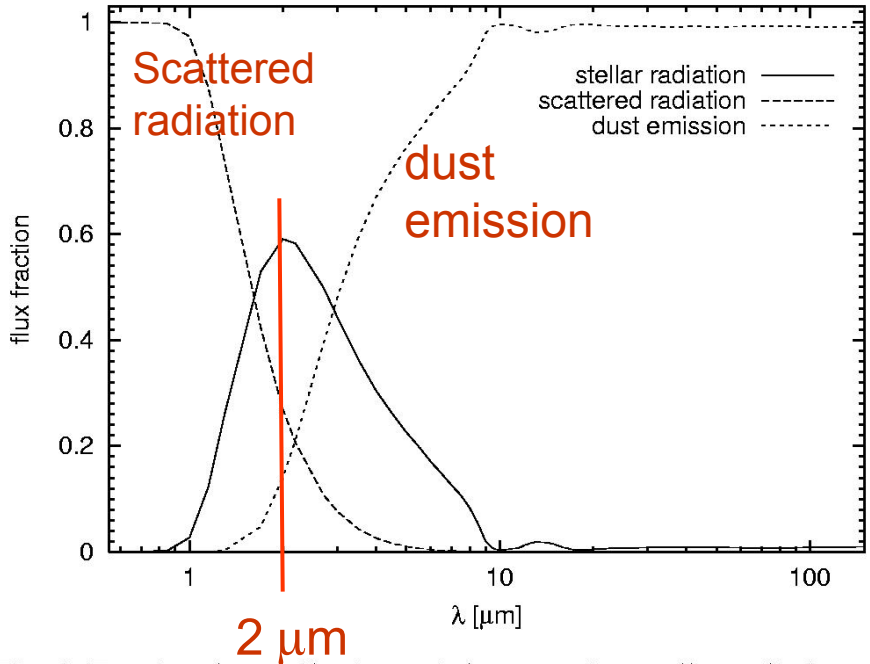

Fig. 4. Fractional contributions of the emerging stellar radiation, the scattered radiation, and of the dust emission to the total flux as a function of the wavelength for a two-component model. The density decreases $\sim 1/r^2$ for $Y_2 \leq 20.5$, and $\sim 1/r^{1.5}$ for $Y_2 > 20.5$. (see Fig. 3). Model parameters are: black body, $T_{\rm eff} = 2250\,{\rm K}$, $T_1 = 900\,{\rm K}$, $\tau_{0.55\mu{\rm m}} = 30$, Ossenkopf et al. (1992) silicates, and a Mathis et al. (1977) grain size distribution with $a_{\rm max} = 0.25\,\mu{\rm m}$.

Dust shell of the AGB star Cit 3: DUSTY radiative transfer modeling

(Hofmann et al. 20001, A&A 379, 529)

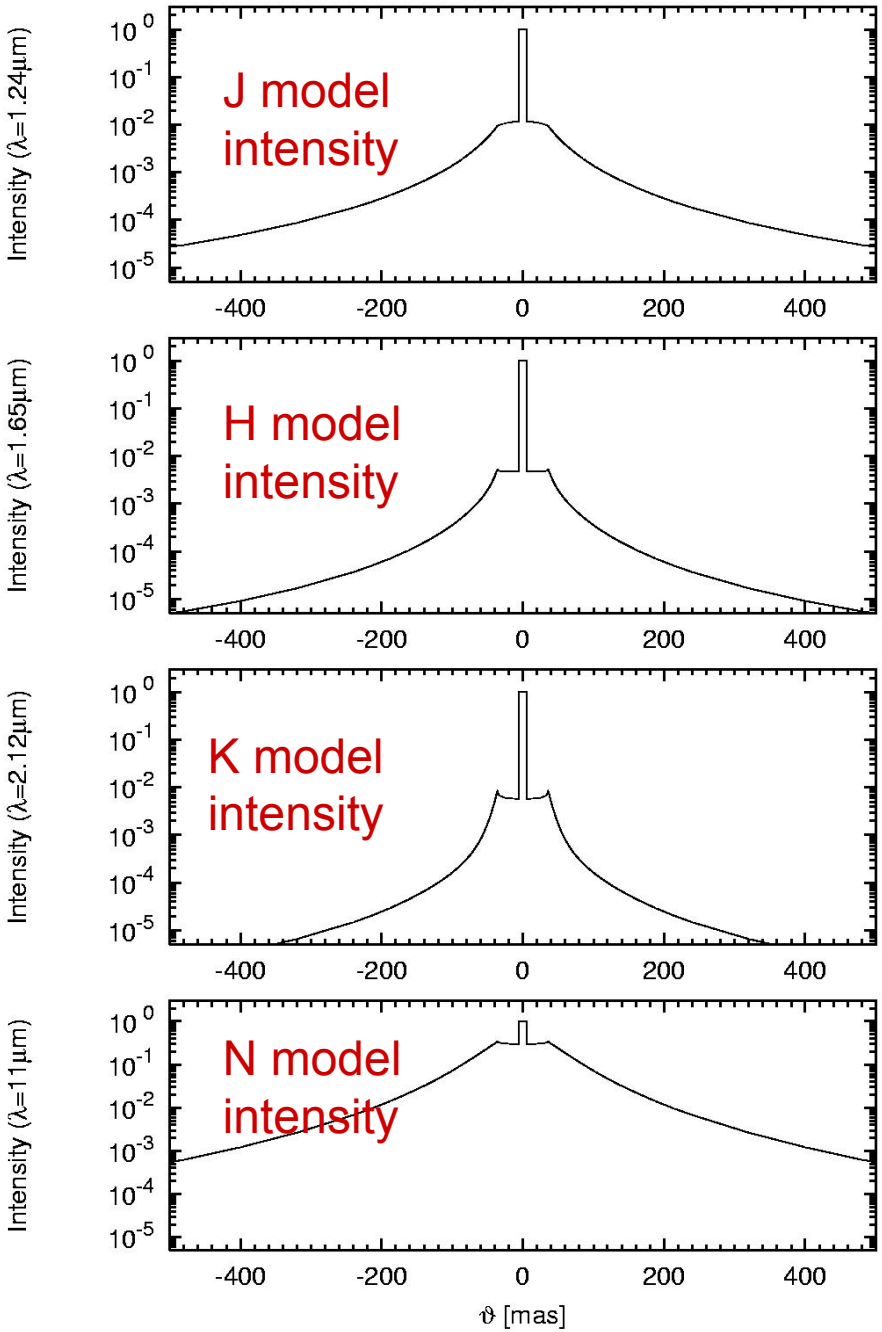

Radiative transfer modeling of the carbon star IRC +10216:

SED
+ *JHK* visibilities
+ *LN* visibilities
+ *JHK* images

(Menshchikov et al. 2002, A&A, 392, 921)

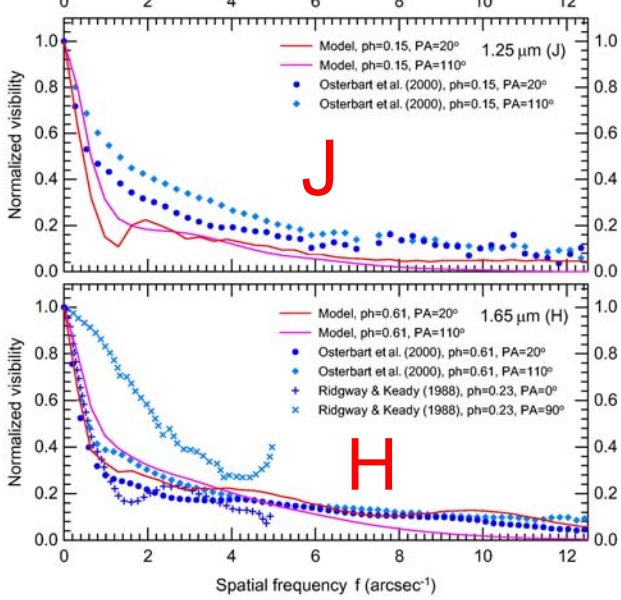

Fig. 24. Model visibilities of IRC +10 216 in J and H bands are plotted for only two orthogonal directions, PA ≈ 20° and PA ≈ 110°. Visibilities from Ridgway & Keady (1988) are also shown, for reference, in the lower panel

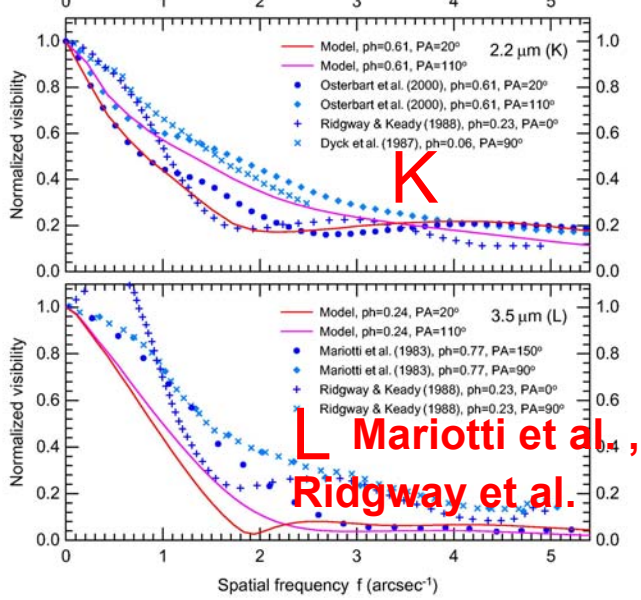

Fig. 26. Model visibilities of IRC +10 216 in K and L bands are plotted for only two orthogonal directions, PA ≈ 20° and PA ≈ 110°. Data at low spatial frequencies may be less reliable (L band, lower panel)

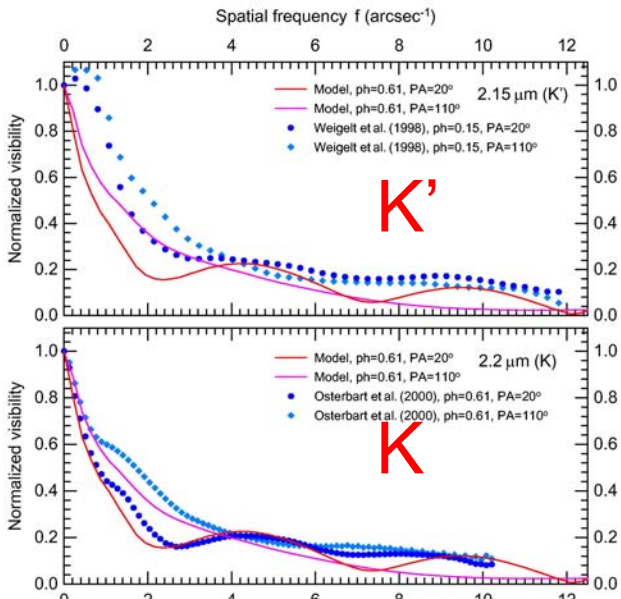

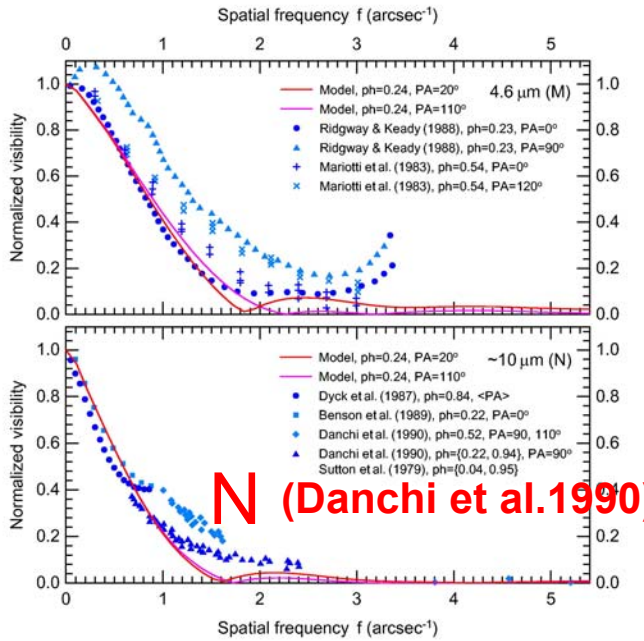

Dust shell of the carbon star IRC+10216:

1995-2003

(Weigelt et al. 2002, A&A 392, 131)

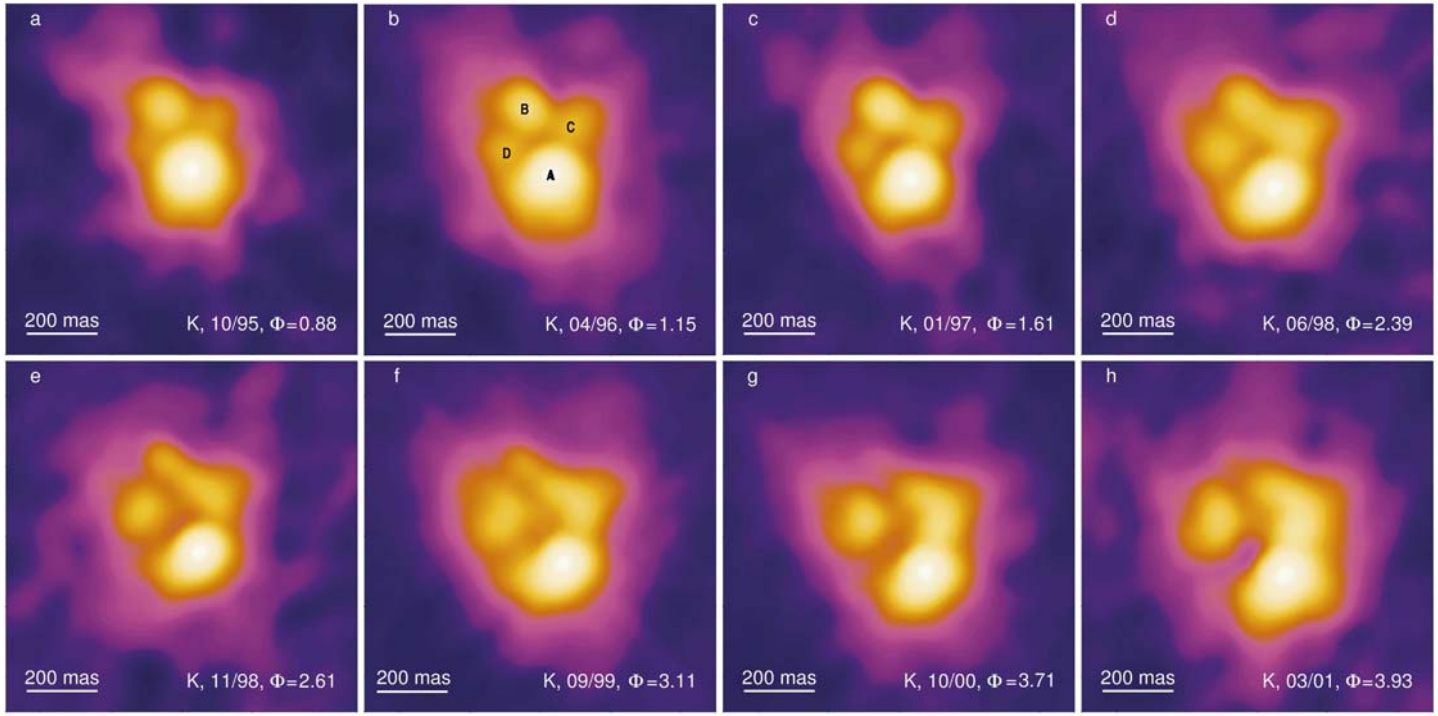

Fig. 1. *K*-band speckle reconstructions of IRC +10216 for 8 epochs from 1995 to 2001. The total area is 1″×1″. All images are normalized to the brightest pixel and are presented with the same color table. North is up and east is to the left.

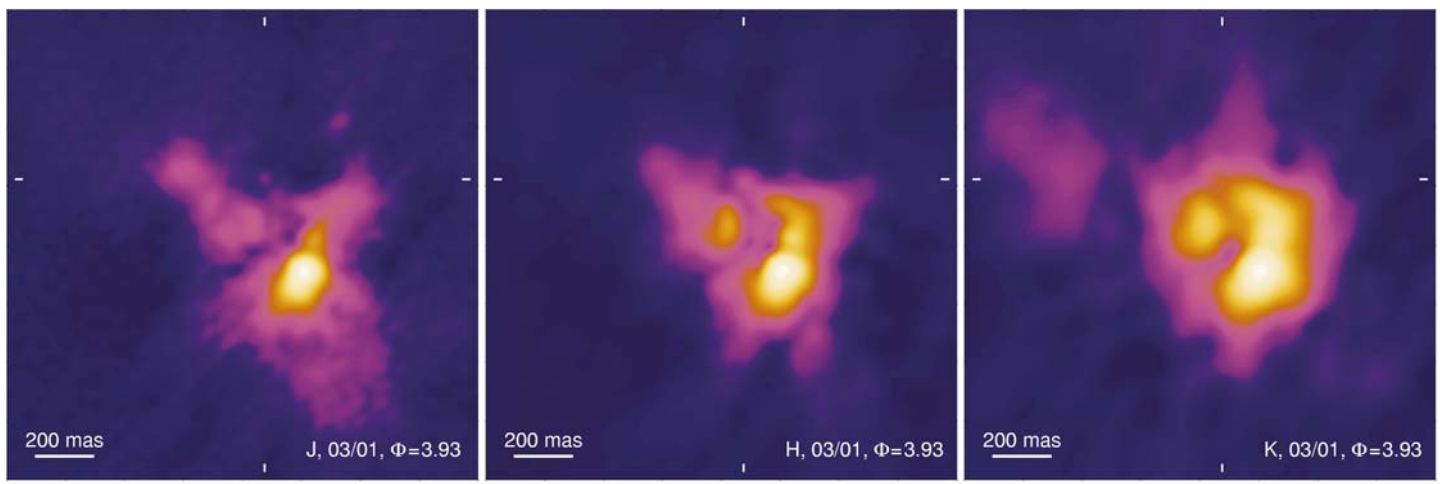

Fig. 2. *J*-, *H*- and *K*-band speckle reconstructions of IRC +10216 in March 2001. The total area is 1.6″×1.6″. All images are normalized to the brightest pixel and are presented with the same color table. North is up and east is to the left. The tick marks indicate the likely position of the central star.

The Red Rectangle – Observations vs. 2D Modeling

6 m telescope (60 mas) KECK (45 mas) KECK

Observations

Models

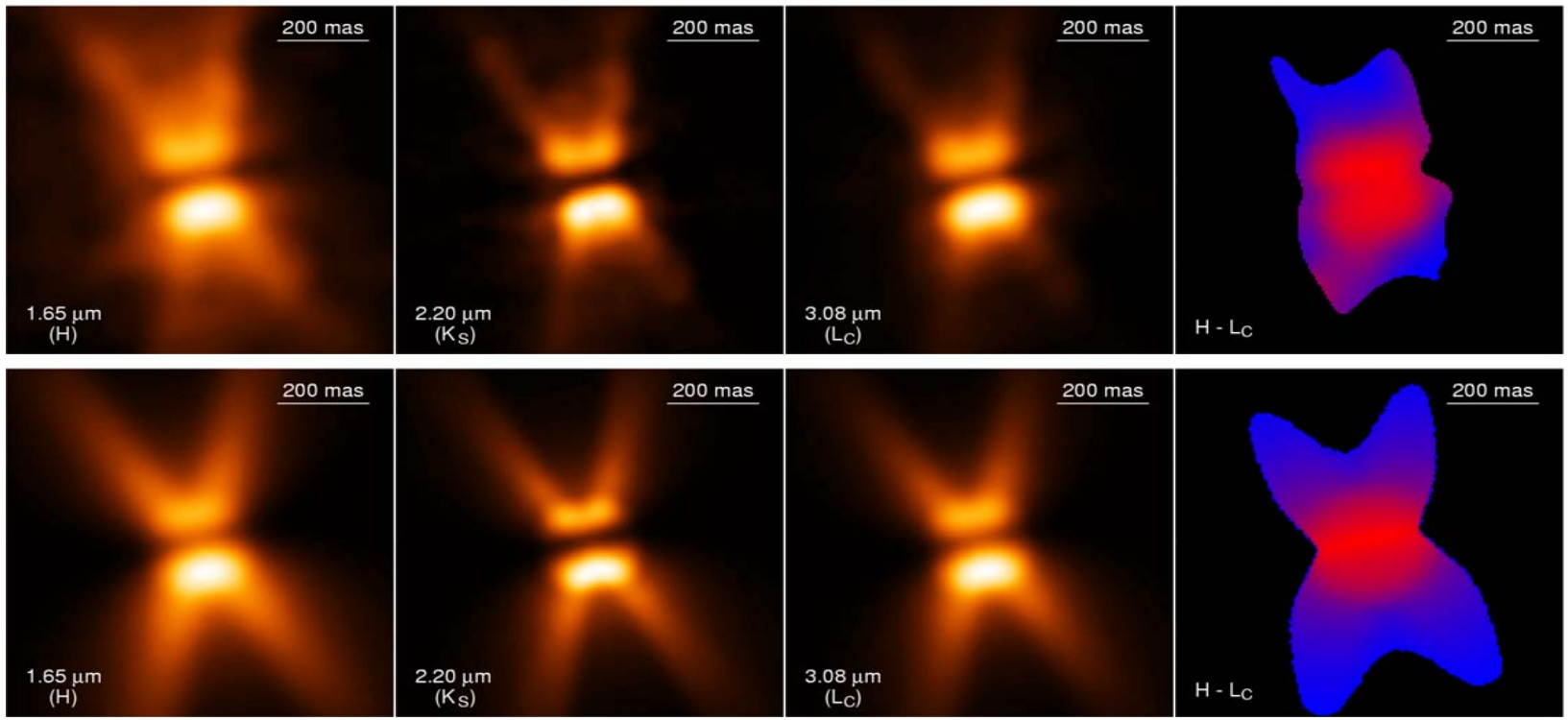

- Our model reproduces the prominent features of the observed images in the IR from 1.65 to 3.08 μm and in the optical regime.
- Biconical shape is preserved from visible to at least mid-IR wavelenghts.

(Tutthill et al. 2003, A&A 389, 889; Menshchikov et al. 2003, A&A 393, 867)

Young massive star AFGL 2591: outflow & dust sublimation radius

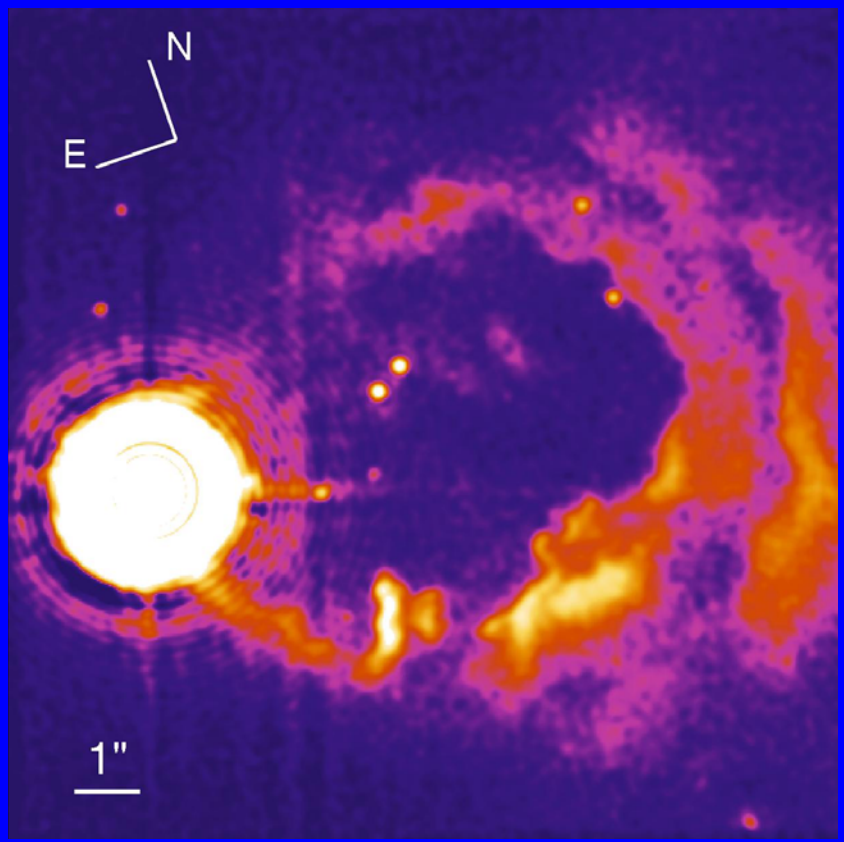

Preibisch et al. 2003

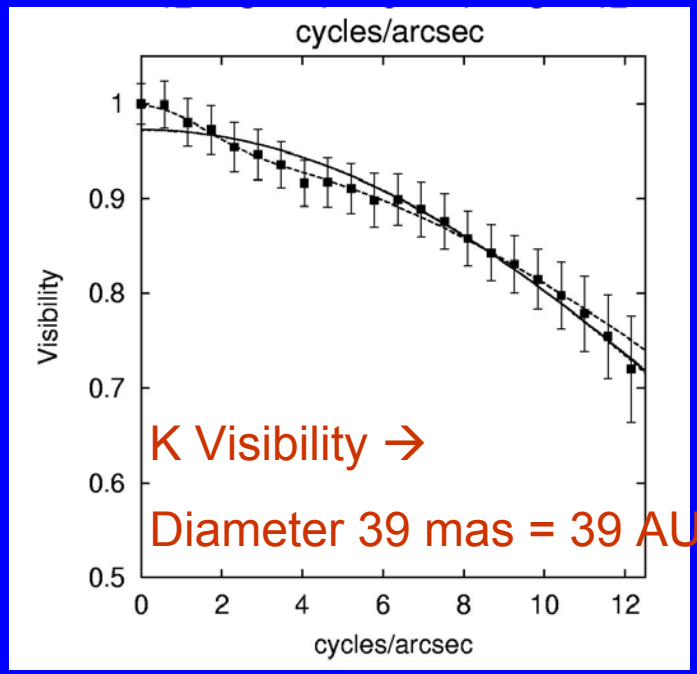

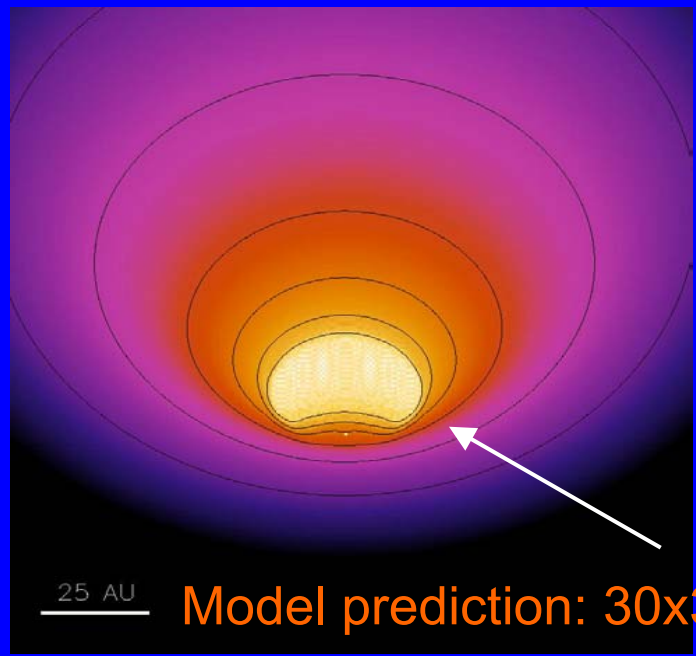

Advantages and aims of NIR interferometry (e.g., VLTI AMBER)

- ***JHK*** + ***N*** visibility + images+ SED:
  2D *JHKN* radiative transfer modeling

- 0.1-1% visibility accuracy:
  Stellar surface structure
  Sublimation radius of dust disks of YSO
  Outflows and jets of YSO
  AGN dust tori

- 0.01% accuracy of differential vis.:
  BLR (diameter ~ 0.1 mas),
  inner region of jets of YSO,
  exo-planets … (talk by R. Petrov)

671 nm TiO:
36x51mas

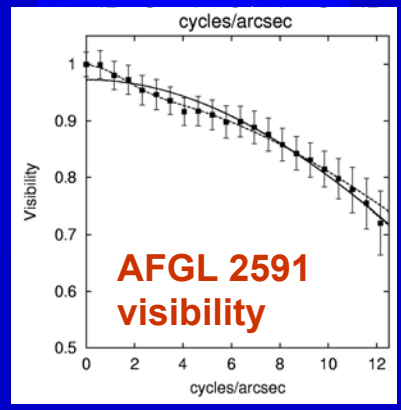

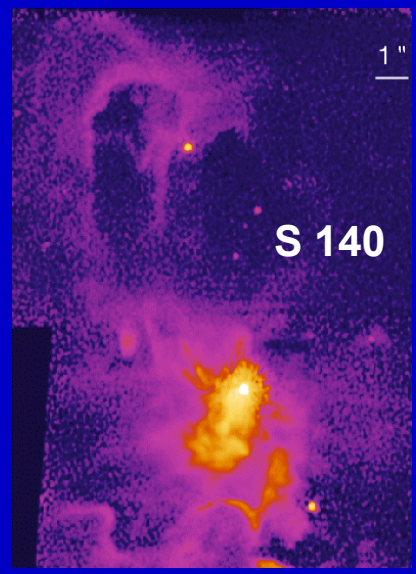

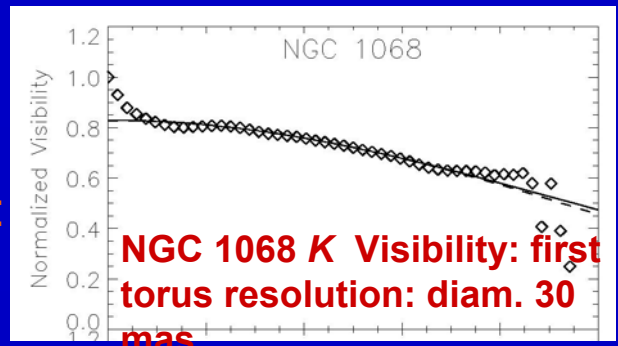

Wittkowski et al. 1998, A&A 329, L49

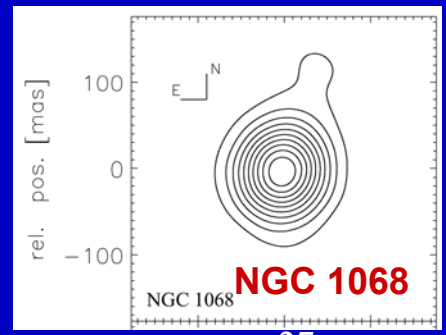

K **image NGC 1068**